Applied Physics Letters ARTICLE scitation.org/journal/apl

Gold atom diffusion assisted thermal healing enabling high-performance hole-transporting material in solar cells

Cite as: Appl. Phys. Lett. **119**, 211904 (2021); doi: 10.1063/5.0067814
Submitted: 19 August 2021 · Accepted: 9 November 2021 ·
Published Online: 23 November 2021

View Online Export Citation CrossMark

Chenhui Jiang,[1,2] Zheng Wang,[1,2] Rongfeng Tang,[1,2] Changfei Zhu,[1,2,a)] Lijian Zhang,[1,2,a)] and Tao Chen[1,2,a)]

AFFILIATIONS

[1]Hefei National Laboratory for Physical Sciences at Microscale, CAS Key Laboratory of Materials for Energy Conversion, Department of Materials Science and Engineering, School of Chemistry and Materials Science, University of Science and Technology of China, Hefei 230026, China
[2]Institute of Energy, Hefei Comprehensive National Science Center, Hefei, China

[a)]**Authors to whom correspondence should be addressed:** cfzhu@ustc.edu.cn; zlijian@mail.ustc.edu.cn; and tchenmse@ustc.edu.cn

ABSTRACT

The use of the compact hole-transporting layer (HTL) with strong hole extraction ability is vital to prepare high-efficiency solar cells. Here, we report the application of 2,3,5,6-tetrafluoro-7,7,8,8-tetracyanoquinodimethane (F4-TCNQ) doped copper phthalocyanine (CuPc) as the hole-transporting layer for the $Sb_2(S,Se)_3$ solar cells. We find that the diffusion of gold atoms into the copper phthalocyanine film is able to heal the cracks and pinholes of the CuPc film, which enables the morphology to become more flat and denser, along with enhanced hole mobility. Benefitting from these results, the F4-TCNQ doped CuPc-based $Sb_2(S,Se)_3$ solar cells achieved best power conversion efficiency of 8.57%. More importantly, the device based on F4-TCNQ doped CuPc HTL showed essentially improved operational stability under the condition of 85% humidity and 85 °C. This research provides a suitable method for improving the morphology and transport properties of the CuPc based hole-transporting layer for solar cell and other optoelectronic device applications.

Antimony selenosulfide [$Sb_2(S,Se)_3$] has emerged as a highly stable light-absorbing material with superior optoelectronic properties, which possesses strong absorption coefficient ($\sim 10^5\,cm^{-1}$) and tunable bandgap in the range of 1.1–1.8 eV through changing the atomic ratio of S/Se.[1,2] In addition, the compositional elements are abundant in Earth and the compound is nontoxic.[3] Due to the potential in practical applications, great efforts have been put into the material and device study. It has been observed that the high-efficiency $Sb_2(S,Se)_3$ solar cells are exclusively based on the organic hole-transporting layer (HTL) with extra hygroscopic dopants. Typically, Spiro-OMeTAD and DTPThMe-ThTPA HTLs have led to the power conversion efficiency (PCE) around 10%.[4–6]

However, the application of hygroscopic dopants and the materials characteristics raise concerns regarding the device stability under moisture and thermal surroundings, which, in turn, poses challenge in the future practical applications.[7,8] In this regard, alternative HTLs that are more stable to moisture and heat are urgently desired for efficient and stable $Sb_2(S,Se)_3$ solar cells. To this end, some inorganic materials, such as V_2O_5,[9] PbS,[10] $CuSbSe_2$,[11] and WO_{3-x},[12] have been developed as HTLs for the antimony chalcogenides solar cells and showed increased stability. However, the PCEs of the devices are unsatisfactory (usually below 8%) because of their relatively low carrier extraction capacity compared with the ones using the doped Spiro-OMeTAD.

Recently, p-type semiconductor copper phthalocyanine (CuPc) and its derivatives are considered as promising HTL candidates because of their outstanding chemical and thermal stability as well as high hole mobility.[13–15] Given these excellent features, CuPc with suitable dopant has been utilized as HTL in perovskite solar cells, which exhibited long-term durability and comparable efficiency with that based on Spiro-OMeTAD HTL.[16,17] Nevertheless, there has been no attempts in the application of CuPc based HTL in inorganic thin film solar cells.

Stimulated by the application in perovskite solar cells, here we applied the CuPc thin film as HTL in $Sb_2(S,Se)_3$ solar cell through spin-coating the chlorobenzene solution of copper(II) 2,9,16,23-tetra-tert-butyl-29*H*,31*H*-phthalocyanine. In specific, to

evaluate the effect of CuPc as HTL on $Sb_2(S,Se)_3$ solar cell performance, we adopted the SnO_2 doped with fluorine (FTO)/CdS/$Sb_2(S,Se)_3$/HTL/Au device structure [Fig. 1(a)], where the CdS as the electron-transporting layer was fabricated by the chemical bath deposition approach and the $Sb_2(S,Se)_3$ absorber layer was fabricated by the hydrothermal deposition method. The CuPc HTL was fabricated by the spin-coating approach. The detailed fabrication process is provided in the experimental section in the supplementary material. The as-prepared device delivers average PCE of 3.77% ± 0.61%, with an open-circuit voltage (V_{OC}) of 599% ± 32% mV, the short-circuit current density (J_{SC}) of 18.53% ± 1.16% mA/cm^2, and fill factor (FF) of 33.76% ± 3.13% [Fig. 1(c), Fig. S1, and Table S1 in the supplementary material]. To improve the interfacial contact, we annealed the device at 85 °C for 24 h in N_2 atmosphere [denoted as CuPc(A)] as shown in Fig. 1(b). Figure 1(c) shows the dependence of PCE on the annealing treatment. Upon post-annealing treatment, surprisingly, all the photovoltaic parameters are dramatically improved, which gives the final efficiency of 7.14% ± 0.22% [Figs. 1(c) and S1]. In order to further improve the device efficiency, we doped 2,3,5,6-tetrafluoro-7,7,8,8-tetracyanoquinodimethane (F4-TCNQ) into CuPc (denoted as F4-CuPc) to lower the lowest unoccupied molecular orbital (LUMO) energy level and enhance the hole-transporting capability.[18,19] It is observed that after doping, there is obvious enhancement in the FF from 33.76% ± 3.13% to 36.40% ± 3.98% (Fig. S1) delivering PCE of 4.43% ± 0.60% for the original device [Fig. 1(c)]. After the same post-annealing as mentioned above [denoted as F4-CuPc(A)], the average PCE jumped to 8.01% ± 0.28% [Figs. 1(c) and S1]. Specially, FF was improved obviously, from 36.40% ± 3.98% to 56.97% ± 2.76%, which is due to the efficient charge extraction upon post-annealing as discussed below.[20,21] Among them, the best device exhibited PCE of 8.57% with V_{OC} of 647 mV, J_{SC} of 23.52 mA/cm^2, and FF of 56.32% [Fig. 1(d)]. The external quantum efficiency (EQE) of the best device can reach greater than 90% in the visible region [Fig. 1(e)]. The integrated J_{SC} value from the EQE curve is 22.3 mA/cm^2, comparable to the value obtained from the *J–V* measurement.

To explore the reason why the post-annealing treatment can improve the device performance, we carried out control experiment by annealing the device of CuPc-based samples before depositing the gold electrode. Afterward, a gold electrode was deposited onto the surface of the CuPc film to complete the device assembly. Figure S2 compares the parameters of the devices without post-annealing, with post-annealing before depositing the gold electrode [i.e., FTO/CdS/$Sb_2(S,Se)_3$/CuPc], and with post-annealing after depositing the gold electrode [i.e., FTO/CdS/$Sb_2(S,Se)_3$/CuPc/Au], which shows clearly that the post-annealing treatment is able to improve the device performance. However, it is not obvious for the PCE improvement in the device fabricated with post-annealing before depositing the gold electrode, which means that the enhancement of PCE does not come from the improvement in the interfacial contact upon the annealing treatment. Only the post-annealing after depositing the gold electrode, i.e., the complete device, can the treatment deliver obvious improvement in V_{oc}, FF, and PCE. Therefore, we hypothesize that gold electrode plays critical role in the device efficiency improvement under the post-annealing treatment.

We then conducted scanning electron microscopy (SEM) examination on the surface morphology change upon post-annealing treatment. As shown in Fig. 2(a), the pristine F4-CuPc HTL deposited on the $Sb_2(S,Se)_3$ surface presents vast and large cracks and pinholes,

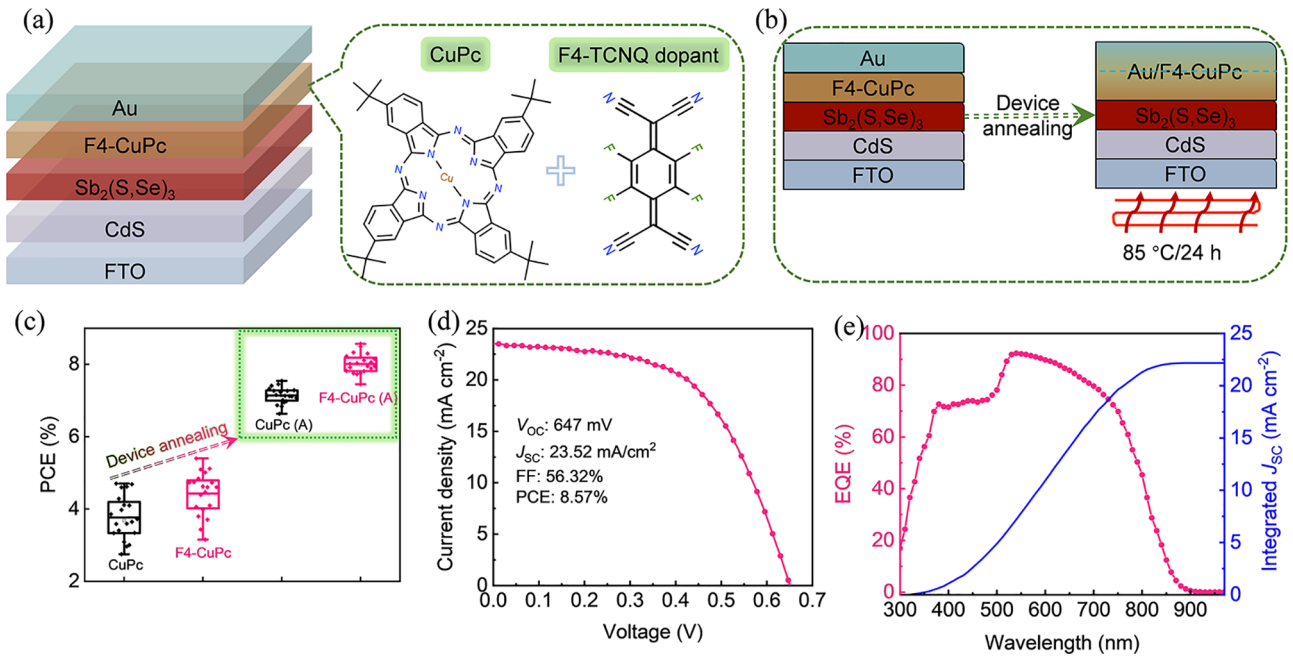

FIG. 1. (a) Device structure diagram and the molecular structures of CuPc and F4-TCNQ. (b) Schematic diagram of device annealing. (c) Statistical PCE distribution of pristine and post-annealing treated $Sb_2(S,Se)_3$ solar cells with CuPc and F4-CuPc as HTLs. (d) *J–V* curve and (e) EQE of the best device based on F4-CuPc HTL after post-annealing treatment.

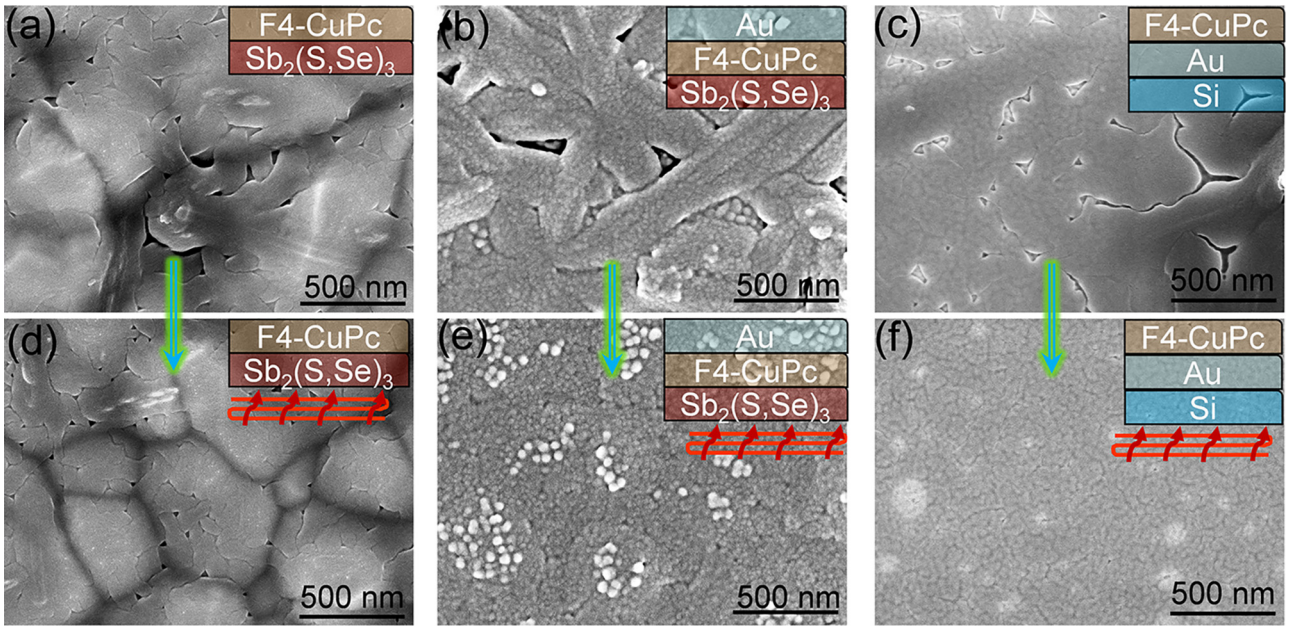

FIG. 2. Surface SEM images of (a) $Sb_2(S,Se)_3$/F4-CuPc, (b) $Sb_2(S,Se)_3$/F4-CuPc/Au, and (c) Si/Au/F4-CuPc without post-annealing treatment. Surface SEM images of (d)–(f) are the corresponding samples with post-annealing treatment at 85 °C for 24 h. The inset in each figure depicts the structure of each sample.

which is detrimental to the device performance because it can induce direct contact between the gold electrode and $Sb_2(S,Se)_3$ and in turn severe carrier recombination and inefficient carrier transport. Interestingly, the large cracks nearly disappeared after annealing at 85 °C for 24 h, although there still remains pinholes in the F4-CuPc surface [Fig. 2(d)]. This morphological change is benefit to the device performance improvement to some extent (Fig. S1).

We also observed that when a gold film with 50 nm thickness was deposited onto the pristine F4-CuPc surface without annealing, the gold film partially covers the underlying layer and partly fills cracks and pinholes in the F4-CuPc film [Fig. 2(b)]. The cracks and pinholes in the underlying F4-CuPc are also very distinct [Fig. 2(b)]. After annealing this sample at 85 °C for 24 h, these cracks and pinholes in both gold film and underlying layer are effectively healed, resulting in a compact and flat F4-CuPc/Au film [Fig. 2(e)]. In order to elucidate the influence of gold on the surface change in F4-CuPc after annealing, we deposited the F4-CuPc film onto the surface of the gold film (50 nm) deposited onto the silicon substrate instead. Similar to the case in F4-CuPc deposited on the $Sb_2(S,Se)_3$ film, large cracks and massive pinholes are apparently observed in the F4-CuPc/Au film [Fig. 2(c)]. Upon the post-annealing treatment, as expected, these cracks and pinholes completely heal [Fig. 2(f)]. Thus, we further confirm that the presence of gold facilitates the formation of compact and flat F4-CuPc film upon thermal treatment, this thermal healing effect is beneficial for the improvement in the hole extraction capability of F4-CuPc HTL.

In organic semiconductors based optoelectronic devices, metal atoms in electrode are found to, in some cases, diffuse from electrode into the organic film under heating or even at room temperature.[22–24] Recent theoretical calculations have also shown that the large electron negativity metal atoms like gold could produce covalent-like bonds with π-orbitals of carbons in the organic layer and prefer to diffuse along the π-conjugated carbon–carbon (C–C) bonds of the organic materials with small barriers less than 0.2 eV.[25,26] We, thus, rationally speculate that the aforesaid thermal healing effect is resulted from gold atoms diffusing into the CuPc organic film with delocalized π-orbitals. Therefore, x-ray photoelectron spectroscopy (XPS) was carried out to verify the gold atoms movement in the experiment. XPS first collected signals from the F4-CuPc film deposited on the ITO substrate with gold electrodes, as shown on the left side of Fig. 3(a). It is expected that Au 4f core-level spectra of the pristine sample cannot be detected [Fig. 3(b)]. Since the detection depth of XPS is only about 10 nm, the thickness of the F4-CuPc film is about 50 nm, which hinders the detection of Au. However, as for the sample after annealing at 85 °C for 24 h, as shown on the right side of Fig. 3(a), the peak located at 84.08 and 87.79 eV corresponding to Au 4f can be detected, indicating that Au appeared near the surface of the F4-CuPc film [Fig. 3(b)]. What is more, the signal intensity of Cu 2p, C 1s, and N 1s of F4-CuPc remains nearly invariable before and after annealing (Fig. S3). Moreover, the binding energies of these elements are found to have no shift as well. These results demonstrate that gold atoms diffused into the F4-CuPc film, and there is no chemical reaction between gold and F4-CuPc film under heat treatment, which promotes the reorganization of HTL to form a flat and dense film. To further determine the diffusion between gold electrode and F4-CuPc before and after annealing, the elemental depth profile was characterized by time-of-flight secondary ion mass spectrometry (ToF-SIMS). As shown in Fig. S4, Au and Cu are selected for identifying the gold electrode and F4-CuPc layer, respectively. For the sample without post-annealing, it is clearly seen that the Au signal starts dropping before the Cu signal being detected. In contrast, as for the sample with post-annealing, the signal peak of Au move to the Cu signal range with improved overlap was detected, which well confirms the diffusion of Au into the F4-CuPc layer.

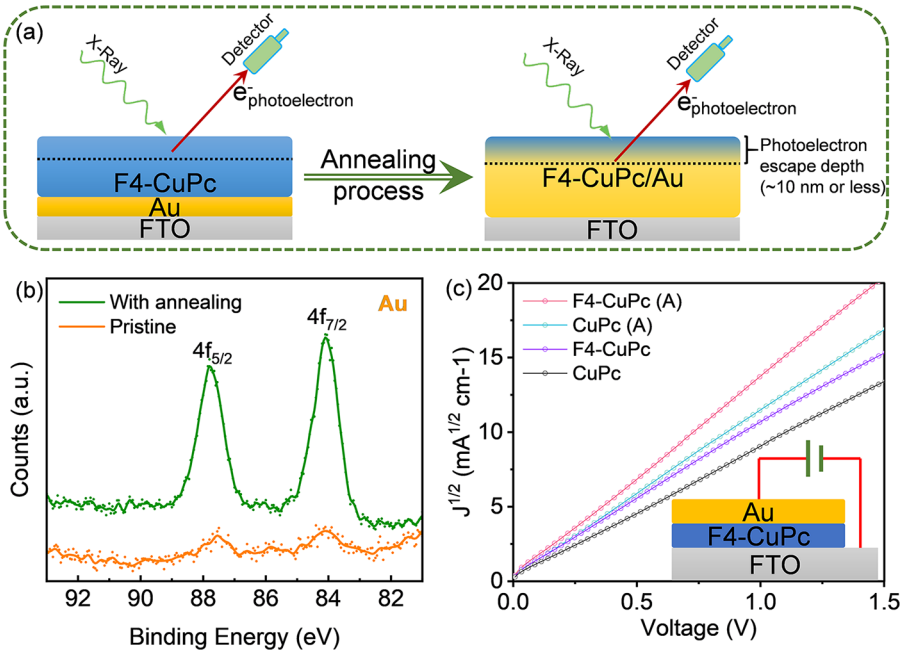

FIG. 3. (a) Schematic diagram of XPS characterization on the surface properties of the films. (b) XPS spectra of Au in the pristine Au/F4-CuPc film and Au/F4-CuPc film with annealing at 85 °C for 24 h. (b) Hole mobility measurements of CuPc, F4-CuPc without and with post-annealing treatment.

The space-charge-limited-current (SCLC) method was then implemented to examine the change in the hole mobility of F4-CuPc HTL with Au before and after post-annealing. The test structure adopts FTO/F4-CuPc/Au, as shown in the inset of Fig. 3(c). The hole mobility of F4-TCNQ doped CuPc is estimated to be 4.14×10^{-4} $cm^2 V^{-1} s^{-1}$, which is higher than the pristine CuPc HTL (2.61×10^{-4} $cm^2 V^{-1} s^{-1}$). However, after annealing, the hole mobility is improved for CuPc (4.12×10^{-4} $cm^2 V^{-1} s^{-1}$) and F4-CuPc (6.46×10^{-4} $cm^2 V^{-1} s^{-1}$). We can readily attribute the improved hole mobility after post-annealing treatment to the enhancement of the conductivity after the diffusion of gold.

The improvement in the morphology and the increase in the mobility could promote the carrier extraction ability of the film. Therefore, we performed femtosecond transient absorption (TA) spectroscopy to study charge carrier dynamics. More detailed experimental procedures for the TA measurement can be found in the supplementary material. Figure S5(a) presents TA pseudocolor image of the FTO/CdS/$Sb_2(S,Se)_3$ sample under excitation by a 400 nm pump laser pulse. The narrow TA negative peak located at ~500 nm corresponds to the ground-state bleaching (GSB) signal of the CdS buffer layer underneath the $Sb_2(S,Se)_3$ film. The broad positive signal located at ~550–700 nm corresponds to the excited-state photoinduced absorption (PIA) signal of the $Sb_2(S,Se)_3$ film coming from the presence of $S^{-\bullet}$ species in the $Sb_2(S,Se)_3$.[5,6,27,28] As the delay time between the pump and probe laser pulse prolongs, the TA signal (ΔA) of the $Sb_2(S,Se)_3$ film gradually decreased, indicating an increased recombination rate between photoinduced electrons and holes in the $Sb_2(S,Se)_3$ [Figs. S4(a) and S4(b)]. Figure S5(c) shows the corresponding relaxation kinetic traces at 635 nm, which could be well fitted with a double exponential function,

$$y = A_1 e^{\frac{-t}{\tau_1}} + A_2 e^{\frac{-t}{\tau_2}},$$

where A_1 and A_2 are prefactors and τ_1 and τ_2 are time constants. The average lifetime τ_{ave} was estimated from the fitting parameters according to the following equation $\tau_{ave} = \Sigma A_i \tau_i 2 / \Sigma A_i \tau$. According to this function, the relevant decay time constants were collected. As shown in Table S2, $Sb_2(S,Se)_3$ undergoes an average decay lifetime of 9263 ps through the electron–hole recombination process. Capping this $Sb_2(S,Se)_3$ film with F4-CuPc HTL, the PIA signal intensity of $Sb_2(S,Se)_3$ decreases to a small extent in the full delay timescale [Fig. 4(a)]. In detail, as depicted in Fig. 4(b), the positive ΔA peak intensity of the $Sb_2(S,Se)_3$/F4-CuPc sample is obviously weaker than that of the $Sb_2(S,Se)_3$ sample at the same delay time of 100 ps, 500 ps, 2 ns, and 5 ns. Extracting from the decay trace of PIA feature, the $Sb_2(S,Se)_3$/F4-CuPc sample shows slightly reduced short (τ_1) and long (τ_2) decay lifetime than the $Sb_2(S,Se)_3$ sample [Fig. 4(c) and Table S2]. It is believed that the transfer of photogenerated charge carrier reduces the population of excited-state charge, which further causes the photo-induced absorption to recover faster.[29] Therefore, the as-prepared F4-CuPc film indeed has the capability of hole extraction from the $Sb_2(S,Se)_3$ light absorbed layer, but the ability is too inferior to create a satisfying device efficiency [Fig. 1(c)].

We further conducted post-annealing treatment of the $Sb_2(S,Se)_3$/F4-CuPc film for the TA characterization [Figs. 4(d)–4(f)]. We find that the lifetime constants of this post-annealing treated $Sb_2(S,Se)_3$/F4-CuPc are shorter than the as-prepared counterpart because of the improvement in the surface morphology of F4-CuPc after annealing [Fig. 2(d)]. Then, an ultrathin gold film with the thickness of about 2 nm was evaporated onto the $Sb_2(S,Se)_3$/F4-CuPc film, following by the identical post-annealing treatment process. As shown in Fig. 4(g), the PIA peak intensity of $Sb_2(S,Se)_3$ decreases in whole delay time scale. Taking the delay time of 100 ps as example, the TA signal intensity of $Sb_2(S,Se)_3$ in the heated F4-CuPc HTL with gold is about half of the heated F4-CuPc HTL without gold. Considering the

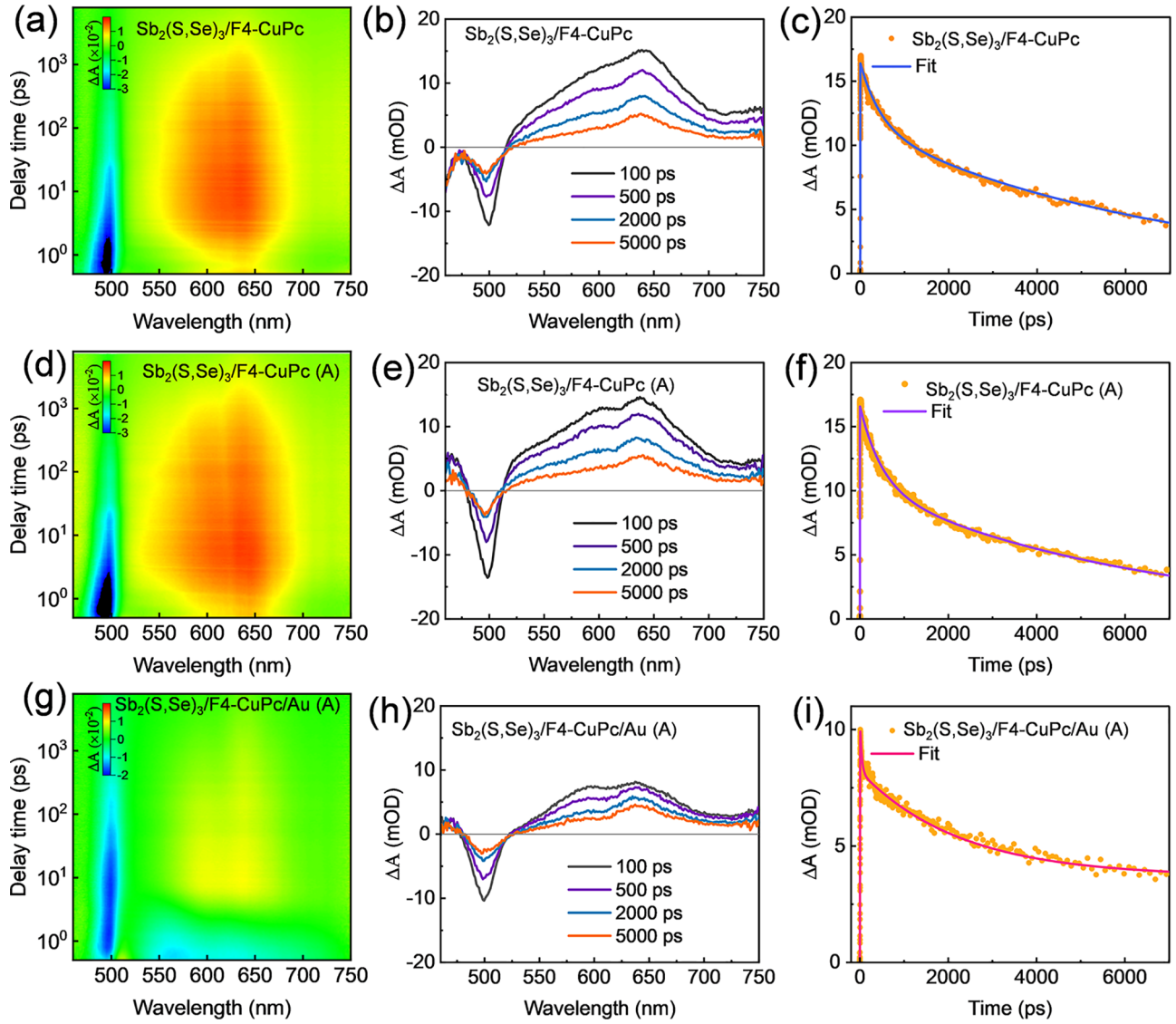

FIG. 4. Transient absorption (TA) characterization of $Sb_2(S,Se)_3$ films. Pseudocolor image of transient response of (a) $Sb_2(S,Se)_3$, (d) $Sb_2(S,Se)_3$/F4-CuPc, (g) post-annealing treated $Sb_2(S,Se)_3$/F4-CuPc, (j) post-annealing treated $Sb_2(S,Se)_3$/F4-CuPc/Au with the 400-nm pump pulse. TA spectra at different delay times of (b) $Sb_2(S,Se)_3$, (e) $Sb_2(S,Se)_3$/F4-CuPc, (h) post-annealing treated $Sb_2(S,Se)_3$/F4-CuPc, (k) post-annealing treated $Sb_2(S,Se)_3$/F4-CuPc/Au. TA dynamics of (c) $Sb_2(S,Se)_3$, (f) $Sb_2(S,Se)_3$/F4-CuPc, (i) post-annealing treated $Sb_2(S,Se)_3$/F4-CuPc, (l) post-annealing treated $Sb_2(S,Se)_3$/F4-CuPc/Au by tracing TA signals at 635 nm. Solid lines are exponential fits of the TA signals, and the raw data are depicted by symbols.

inferior efficiency of the as-fabricated device and then prominently boosting PCE after heating treatment [Fig. 1(c)], the diffusion of gold into F4-CuPc HTL induced by heat significantly enhances the hole-transporting from $Sb_2(S,Se)_3$ to F4-CuPc HTL and, thus, contributes to the declined PIA signal intensity. In terms of carrier dynamics, the lifetime of the sample deposited gold after annealing decreases ~11-fold in short decay time constant ($\tau_1 = 32$ ps) and ~2.8-fold in long decay time constant ($\tau_2 = 2270$ ps), respectively, indicating the markedly enhanced hole extraction and transport capacity of post-annealing treated F4-CuPc HTL deposited gold electrode beforehand. The same phenomena and results are also found in the CuPc counterpart with gold and thermal treatment as well (Fig. S6 and Table S2). In addition, it should be more noteworthy that the hole transport capability of F4-TCNQ-doping CuPc is increased as evidenced by the reduced decay time constant. As a result, F4-TCNQ is an effective dopant in CuPc HTL and could boost the device performance.

Finally, we examine the device stability based on F4-CuPc and Spiro-OMeTAD HTLs without any encapsulation under severe condition with 85% relative humidity at 85 °C. The normalized V_{OC}, J_{SC}, FF, and PCE are shown in Fig. 5. For the device with Spiro-OMeTAD,

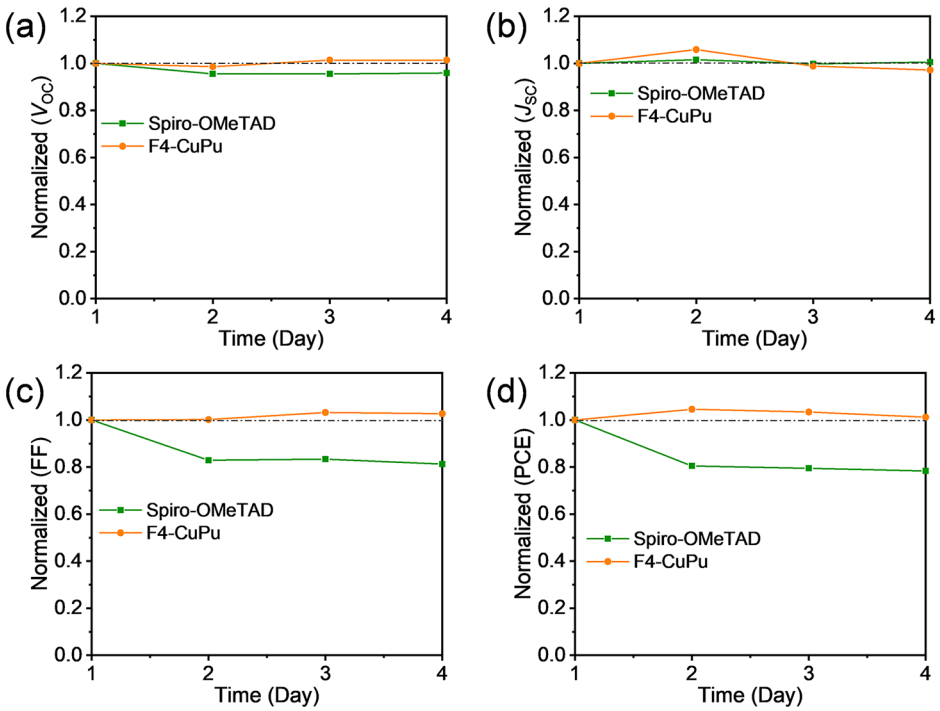

FIG. 5. Normalized (a) V_{OC}, (b) J_{SC}, (c) FF, (d) and PCE of $Sb_2(S,Se)_3$ solar cells based on F4-CuPc and Spiro-OMeTAD HTLs as a function of storage time at the condition of 85% relative humidity and 85 °C.

there is serious reduction in V_{OC} and FF [Figs. 5(a) and 5(c)], this change may be due to the deliquescent behavior of the doped Spiro-OMeTAD in the humidity environment, which would increase the series resistance.[30] The overall PCE of the device with Spiro-OMeTAD as HTL decreased to 80% of its initial efficiency after four days in this condition, whereas all devices based on F4-CuPc HTL show excellent stability and almost no reduction in efficiency compared with the initial efficiency. Therefore, the substitution of Spiro-OMeTAD for F4-CuPc layers leads to substantially improved device stability.

In summary, we have demonstrated that F4-TCNQ doped CuPc can serve as an efficient hole-transporting layer for $Sb_2(S,Se)_3$ based solar cells. We found that the diffusion of gold atom from the electrode into the F4-TCNQ doped CuPc film was able to heal the cracks and holes within the film and, in turn, generate more flat and dense morphology. These improvements resulted in essentially enhanced hole mobility. Benefitting from these results, the best F4-TCNQ doped CuPc-based $Sb_2(S,Se)_3$ solar cells achieved a PCE value of 8.57%. Furthermore, the device based on F4-TCNQ doped CuPc HTL showed essentially improved operational stability compared with the conventional device based on the organic hole transporting layer. This study suggests that F4-TCNQ-doped CuPc is a promising hole-transporting material, and a proper post-annealing treatment is critical for obtaining high-efficiency solar cells.

See the supplementary material for (1) materials and methods in detail; (2) table of photovoltaic parameters; (3) table of delay time constants of transient absorption; and (4) the corresponding other experimental date.

This work was supported by National Key Research and Development Program of China (No. 2019YFA0405600), Institute of Energy, Hefei Comprehensive National Science Center (No. 21KZS212), National Natural Science Foundation of China (Nos. U19A2092 and GG2060140111), and Collaborative Innovation Program of Hefei Science Center, CAS.

AUTHOR DECLARATIONS

Conflict of Interest

The authors declare no conflict of interest.

Author Contributions

C.J. and Z.W. contributed equally to this work.

DATA AVAILABILITY

The data that support the findings of this study are available from the corresponding authors upon reasonable request.

REFERENCES

[1]R. Kondrotas, C. Chen, and J. Tang, Joule **2**(5), 857 (2018).
[2]C. Chen and J. Tang, ACS Energy Lett. **5**(7), 2294 (2020).
[3]H. Lei, J. Chen, Z. Tan, and G. Fang, Sol. RRL **3**(6), 1900026 (2019).
[4]X. Wang, R. Tang, C. Jiang, W. Lian, H. Ju, G. Jiang, Z. Li, C. Zhu, and T. Chen, Adv. Energy Mater. **10**, 2002341 (2020).
[5]R. Tang, X. Wang, W. Lian, J. Huang, Q. Wei, M. Huang, Y. Yin, C. Jiang, S. Yang, G. Xing, S. Chen, C. Zhu, X. Hao, M. A. Green, and T. Chen, Nat. Energy **5**, 587 (2020).
[6]C. Jiang, J. Zhou, R. Tang, W. Lian, X. Wang, X. Lei, H. Zeng, C. Zhu, W. Tang, and T. Chen, Energy Environ. Sci. **14**(1), 359 (2021).

[7]M. I. D. Neha Arora, A. Hinderhofer, N. Pellet, F. Schreiber, S. M. Zakeeruddin, and M. Grätze, Science **358**, 768 (2017).
[8]S. N. Habisreutinger, T. Leijtens, G. E. Eperon, S. D. Stranks, R. J. Nicholas, and H. J. Snaith, Nano Lett. **14**(10), 5561 (2014).
[9]L. Zhang, C. Jiang, C. Wu, H. Ju, G. Jiang, W. Liu, C. Zhu, and T. Chen, ACS Appl. Mater. Interfaces **10**(32), 27098 (2018).
[10]C. Chen, L. Wang, L. Gao, D. Nam, D. Li, K. Li, Y. Zhao, C. Ge, H. Cheong, H. Liu, H. Song, and J. Tang, ACS Energy Lett. **2**(9), 2125 (2017).
[11]Q. Cang, H. Guo, X. Jia, H. Ning, C. Ma, J. Zhang, N. Yuan, and J. Ding, Sol. Energy **199**, 19 (2020).
[12]C. Liu, K. Shen, D. Lin, Y. Cao, S. Qiu, J. Zheng, F. Bao, Y. Gao, H. Zhu, Z. Li, and Y. Mai, ACS Appl. Mater. Interfaces **12**(34), 38397 (2020).
[13]H. Xu, R. Chen, Q. Sun, W. Lai, Q. Su, W. Huang, and X. Liu, Chem. Soc. Rev. **43**(10), 3259 (2014).
[14]J. Xue, S. Uchida, B. P. Rand, and S. R. Forrest, Appl. Phys. Lett. **85**(23), 5757 (2004).
[15]F. Zhang, X. Yang, M. Cheng, W. Wang, and L. Sun, Nano Energy **20**, 108 (2016).
[16]W. Ke, D. Zhao, C. R. Grice, A. J. Cimaroli, G. Fang, and Y. Yan, J. Mater. Chem. A **3**(47), 23888 (2015).
[17]X. Liu, Y. Wang, E. Rezaee, Q. Chen, Y. Feng, X. Sun, L. Dong, Q. Hu, C. Li, and Z.-X. Xu, Sol. RRL **2**(7), 1800050 (2018).
[18]H. Kwon, J. W. Lim, J. Han, L. N. Quan, D. Kim, E. S. Shin, E. Kim, D. W. Kim, Y. Y. Noh, I. Chung, and D. H. Kim, Nanoscale **11**(41), 19586 (2019).
[19]Y. Xiong, L. Ye, A. Gadisa, Q. Zhang, J. J. Rech, W. You, and H. Ade, Adv. Funct. Mater. **29**(1), 1806262 (2019).
[20]A. Abdolahzadeh Ziabari, N. Mohabbati Zindanlou, J. Hassanzadeh, S. Golshahi, and A. Bagheri Khatibani, J. Alloys Compd. **842**, 155741 (2020).
[21]J. Peng, D. Walter, Y. Ren, M. Tebyetekerwa, Y. Wu, T. Duong, Q. Lin, J. Li, T. Lu, and M. A. J. S. Mahmud, Science **371**(6527), 390 (2021).
[22]Y. Hirose, A. Kahn, V. Aristov, and P. Soukiassian, Appl. Phys. Lett. **68**(2), 217 (1996).
[23]S. Cacovich, L. Cina, F. Matteocci, G. Divitini, P. A. Midgley, A. D. Carlo, and C. Ducati, Nanoscale **9**(14), 4700 (2017).
[24]M. Scharnberg, J. Kanzow, K. Rätzke, R. Adelung, F. Faupel, S. Meyer, and J. Pflaum, MRS Online Proc. Libr. **871**, I6.31 (2005).
[25]Y. Tomita and T. Nakayama, Appl. Phys. Express **3**(9), 091601 (2010).
[26]Y. Tomita and T. Nakayama, *Electronic Processes in Organic Electronics* (Springer, 2015), p. 303.
[27]C. M. Wolff, P. D. Frischmann, M. Schulze, B. J. Bohn, R. Wein, P. Livadas, M. T. Carlson, F. Jäckel, J. Feldmann, F. Würthner, and J. K. Stolarczyk, Nat. Energy **3**(10), 862 (2018).
[28]J. A. Christians, D. T. Leighton, and P. V. Kamat, Energy Environ. Sci. **7**(3), 1148 (2014).
[29]J. A. Christians and P. V. Kamat, ACS Nano **7**, 7967 (2013).
[30]J. Liu, Y. Wu, C. Qin, X. Yang, T. Yasuda, A. Islam, K. Zhang, W. Peng, W. Chen, and L. Han, Energy Environ. Sci. **7**(9), 2963 (2014).